applied sciences

MDPI

Article

Noninvasive In Vivo Estimation of *HbA1c* Based on the Beer–Lambert Model from Photoplethysmogram Using Only Two Wavelengths

Mrinmoy Sarker Turja [1], Tae-Ho Kwon [1], Hyoungkeun Kim [2] and Ki-Doo Kim [1,*]

[1] Department of Electronics Engineering, Kookmin University, Seoul 02707, Republic of Korea; mrinmoyturja@kookmin.ac.kr (M.S.T.); kmjkth@kookmin.ac.kr (T.-H.K.)
[2] Korea I.T.S. Co., Ltd., Gangnam, Seoul 06373, Republic of Korea; hkkim@koreaits.com
* Correspondence: kdk@kookmin.ac.kr

Abstract: Glycated hemoglobin (*HbA1c*) is the most important factor in diabetes control. Since *HbA1c* reflects the average blood glucose level over the preceding three months, it is unaffected by a patient's activity level or diet before a test. Noninvasive *HbA1c* measurement reduces both the pain and complications associated with fingertip piercing to collect blood. Photoplethysmography is helpful for measuring *HbA1c* without blood samples. Herein, only two wavelengths (615 and 525 nm) were used to estimate *HbA1c* noninvasively, where two different ratio calibrations were applied and their performances were compared to a work that used three wavelengths. For the fingertip type, the Pearson's r values for *HbA1c* estimates were 0.896 and 0.905, considering the ratio calibrations for the blood vessel and whole finger models, respectively. Using another value (*HbA1c*) calibration in addition to the ratio calibrations, we could improve this performance such that the Pearson's r values of the *HbA1c* levels were 0.929 and 0.930 for the blood vessel and whole finger models, respectively. In a previous study, using three wavelengths, the Pearson's r values were 0.916 and 0.959 for the blood vessel and whole finger models, respectively. Here, the RCF of the SpO_2 estimation was 0.986 when the SpO_2 ratio calibration was applied, while in a previous study, the RCF values of the SpO_2 estimation were 0.983 and 0.986 for the blood vessel and whole finger models, respectively. Thus, we have shown that *HbA1c* estimation using only two wavelengths has a comparable performance to previous studies.

Keywords: glycated hemoglobin; *HbA1c*; diabetes; noninvasive; photoplethysmography

Citation: Turja, M.S.; Kwon, T.-H.; Kim, H.; Kim, K.-D. Noninvasive In Vivo Estimation of *HbA1c* Based on the Beer–Lambert Model from Photoplethysmogram Using Only Two Wavelengths. *Appl. Sci.* **2023**, *13*, 3626. https://doi.org/10.3390/app13063626

Academic Editors: Alberto Belli, Paola Pierleoni and Sara Raggiunto

Received: 10 February 2023
Revised: 10 March 2023
Accepted: 10 March 2023
Published: 12 March 2023

1. Introduction

Traditional blood glucose testing often requires blood samples, which can be uncomfortable for a patient and increase the risk of skin and red-blood-cell-life abnormalities. On the other hand, the glycated hemoglobin (*HbA1c*) value reflects the average blood glucose level over the previous three months, and it is unaffected by physical activity or food intake for several hours leading up to measurement. High levels of *HbA1c* indicate poor blood glucose control. As a result, it is used as the most fundamental indicator of the degree of blood glucose control over a period of time and to predict the onset of long-term issues due to diabetes. Human blood consists of 55% yellow liquid plasma, 44% solid red blood cells, and 1% white blood cells and platelets. Hemoglobin is a type of protein found in the red blood cells that plays an important role in transporting oxygen by binding to the oxygen in the blood and to the glucose contained in blood cells. Hemoglobin bound to glucose is called glycated hemoglobin. Regarding glycated hemoglobin, the more glucose there is in the blood, the more the hemoglobin in the red blood cells that binds to the glucose, resulting in higher blood glucose levels. The glycated hemoglobin level is the ratio of glycated hemoglobin to total hemoglobin in the blood. Because the normal lifespan of red blood cells is approximately 4 months and the lifespan of individual red blood cells can

vary widely, this test can only provide the *HbA1c* estimate over the preceding 3 months. People with diabetes are at increased risk of developing additional medical complications, such as heart diseases, kidney failure, stroke, cataracts, and/or premature death. Therefore, the early diagnosis of diabetes in the prediabetic stage is crucial for preventing deterioration of the blood sugar regulation system. This can be achieved through various blood-based tests, such as the random, oral, and fasting blood glucose tests or the glycated hemoglobin (*HbA1c*) test. These tests are used to detect the levels of glucose in the blood, which is a key indicator of diabetes. In diagnosing diabetes, the *HbA1c* test is known to have a better performance than the plasma glucose test [1].

Many enzymatic and nonenzymatic electrochemical glucose sensors [2–7] have been created over the past few decades; however, these approaches are invasive. Immunoassay, ion-exchange high-performance liquid chromatography (HPLC), boronated affinity chromatography, and capillary electrophoresis (CE) are the four most commonly used methods for estimating *HbA1c* [8]. Both HPLC-electrospray mass spectrometry (HPLC-ESI/MS) and HPLC-capillary electrophoresis-ultraviolet (HPLC-CE-UV) are recommended by the International Federation on Clinical Chemistry and Laboratory Medicine (IFCC) for measuring *HbA1c* levels in human blood [9]. All of these methods still require blood samples. However, the development and practical use of noninvasive *HbA1c* estimation tests have been of increasing interest recently. One study [10] only addressed photoplethysmography (PPG) sensor design and did not consider noninvasive in vivo estimation techniques while discussing the estimation of in vitro *HbA1c* levels. Based on the measurement conditions related to hyperglycemia, researchers have divided mouse models into diabetic, obese, and normal control categories [11]. In [12], the authors reported that individuals could be divided into diabetic and non-diabetic categories using PPG signals. In another study [13], the *HbA1c* levels were calculated by also taking into account the acetone levels in the breath. In our previous study [14], we estimated *HbA1c* noninvasively using the Beer–Lambert law-based model with three wavelengths. However, the three wavelengths used made the model complicated and inconvenient for the user, as well. To address these issues, a noninvasive estimation strategy using PPG signals with only two wavelengths is proposed herein. In this study, we used a white LED to provide signals at three wavelengths (465, 525, and 615 nm); of these, red (615 nm) and green (525 nm) were selected to prove the proposed method. Although any two of the three wavelengths can be used, the essence of this study did not change, and a detailed explanation for choosing the wavelength pair (525 and 615 nm) is given in Appendix A.

2. Background

2.1. Beer–Lambert Law

The Beer–Lambert law specifies the attenuation of light passing through a sample [15]. In most cases, the Beer–Lambert law is suitable for quantifying the concentration of a compound remaining in a sample. Accordingly, the attenuation of light is directly proportional to the concentration of the residual compounds in the sample. The practical expression of the Beer–Lambert law is given in Equation (1):

$$A = \varepsilon \times c \times d \,, \tag{1}$$

where A is the total absorption, ε is the molar absorption coefficient ($L \cdot mol^{-1} \cdot cm^{-1}$), c is the concentration of the attenuating species ($mol \cdot cm^{-1}$), and d is the optical path length (cm). Equation (1) can also be expressed in terms of the incident light intensity on the sample and the transmitted light intensity through the sample, as follows:

$$A = \log \frac{I_0}{I} \,, \tag{2}$$

where I_0 is the intensity of light incident on the sample and I is the intensity of the transmitted light through the sample.

2.2. Finger Type Models: Blood Vessel and Whole Finger Models

2.2.1. Blood Vessel Model

The blood vessel model was created using the assumption that the diameter of a vessel increases slightly to accommodate the volume of blood as it enters the vessel and decreases as the blood leaves the channel. This is illustrated in Figure 1.

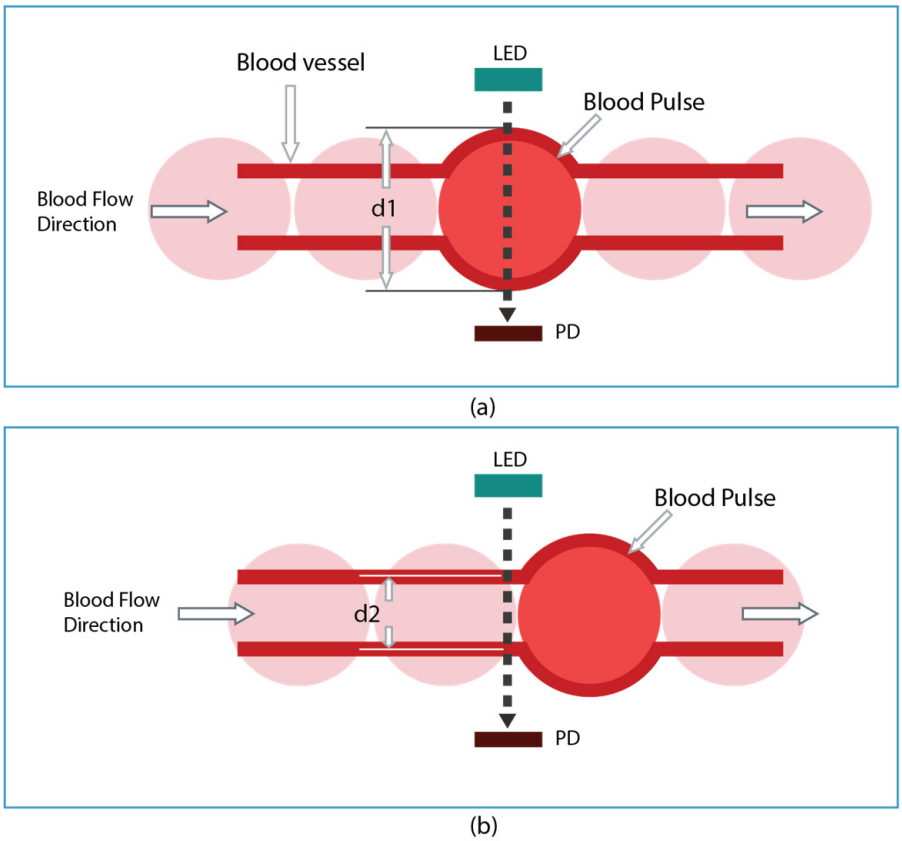

Figure 1. Blood vessel model: (**a**) light intensity in the systolic phase, and (**b**) light intensity in the diastolic phase.

Considering Equation (1), blood can be defined as a homogeneous solution of *HbA1c*, *HbO*, and *HHb*. Hence, the total absorption at wavelength λ can be expressed as

$$A = (\varepsilon_{HbA1c}(\lambda) \times c_{HbA1c} + \varepsilon_{HbO}(\lambda) \times c_{HbO} + \varepsilon_{HHb}(\lambda) \times c_{HHb}) \times d, \quad (3)$$

where $\varepsilon_{HbO}(\lambda)$, $\varepsilon_{HHb}(\lambda)$, and $\varepsilon_{HbA1c}(\lambda)$ are the molar absorption coefficients at the wavelengths λ for *HbO* (oxygenated hemoglobin), *HHb* (deoxygenated hemoglobin), and *HbA1c*, respectively, and c represents the molar concentration of each element while d is the distance traveled by light.

The formulas for $\%SpO_2$ and $\%HbA1c$ can be described as follows:

$$\%SpO_2 = \frac{c_{Hbo}}{c_{HbO} + c_{HHb}} \times 100\% \text{ and} \quad (4)$$

$$\%HbA1c = P_{HbA1c} \times 100\% \,. \quad (5)$$

The partial molar concentrations of *HbO*, *HHb*, and *HbA1c* can be expressed as P_{HbO}, P_{HHb}, and P_{HbA1c}, respectively, as follows:

$$P_{HbO} = \frac{c_{HbO}}{c_T}, \quad (6)$$

$$P_{HHb} = \frac{c_{HHb}}{c_T}, \tag{7}$$

$$P_{HbA1c} = \frac{c_{HbA1c}}{c_T}, \text{ and} \tag{8}$$

$$c_T = c_{HbO} + c_{HHb} + c_{HbA1c}. \tag{9}$$

From Equations (6)–(9),

$$P_{HHb} = 1 - (P_{HbO} + P_{HbA1c}). \tag{10}$$

Equation (4) can be expressed in terms of the partial molar concentration as follows:

$$\%SpO_2 = \frac{P_{Hbo}}{P_{HbO} + P_{HHb}} \times 100\% \,. \tag{11}$$

When the blood vessel expands, Equation (3) becomes

$$\Delta A = (\varepsilon_{HbO}(\lambda) \times c_{HbO} + \varepsilon_{HHb}(\lambda) \times c_{HHb} + \varepsilon_{HbA1c}(\lambda) \times c_{HbA1c}) \times \Delta d, \tag{12}$$

where $\Delta A = A1 - A2$ and $\Delta d = d_1 - d_2$; $A1$ represents the absorbance when blood enters the vessel; and $A2$ represents the absorbance when the blood flows out from the vessel. The variables d_1 and d_2 represent the diameters of the blood vessel as blood enters and leaves the vessel, respectively.

For the two wavelengths considered in this study (i.e., $\lambda 1$ = 525 nm and $\lambda 2$ = 615 nm), Equation (12) can be expressed as

$$\Delta A_{\lambda 1} = (\varepsilon_{HbO}(\lambda 1) \times c_{HbO} + \varepsilon_{HHb}(\lambda 1) \times c_{HHb} + \varepsilon_{HbA1c}(\lambda 1) \times c_{HbA1c}) \times \Delta d \tag{13}$$

$$\Delta A_{\lambda 2} = (\varepsilon_{HbO}(\lambda 2) \times c_{HbO} + \varepsilon_{HHb}(\lambda 2) \times c_{HHb} + \varepsilon_{HbA1c}(\lambda 2) \times c_{HbA1c}) \times \Delta d. \tag{14}$$

From Equations (13) and (14), a ratio equation can be obtained to estimate the unknown parameter P_{HbA1c}. The ratio equation can be expressed as

$$R = \frac{\Delta A_{\lambda 2}}{\Delta A_{\lambda 1}} = \frac{(\varepsilon_{HbO}(\lambda 2) \times c_{HbO} + \varepsilon_{HHb}(\lambda 2) \times c_{HHb} + \varepsilon_{HbA1c}(\lambda 2) \times c_{HbA1c}) \times \Delta d}{(\varepsilon_{HbO}(\lambda 1) \times c_{HbO} + \varepsilon_{HHb}(\lambda 1) \times c_{HHb} + \varepsilon_{HbA1c}(\lambda 1) \times c_{HbA1c}) \times \Delta d} \,. \tag{15}$$

Replacing the molar concentration with the partial molar concentration, we obtain

$$R = \frac{\Delta A_{\lambda 2}}{\Delta A_{\lambda 1}} = \frac{(\varepsilon_{HbO}(\lambda 2) \times P_{HbO} + \varepsilon_{HHb}(\lambda 2) \times P_{HHb} + \varepsilon_{HbA1c}(\lambda 2) \times P_{HbA1c})}{(\varepsilon_{HbO}(\lambda 1) \times P_{HbO} + \varepsilon_{HHb}(\lambda 1) \times P_{HHb} + \varepsilon_{HbA1c}(\lambda 1) \times P_{HbA1c})} \,. \tag{16}$$

Equations (13) and (14) can be expressed in the form of Equation (2) as follows:

$$\Delta A_{\lambda 1} = \Delta \left[\log \frac{I_0}{I} \right]_{\lambda 1} \text{ and} \tag{17}$$

$$\Delta A_{\lambda 2} = \Delta \left[\log \frac{I_0}{I} \right]_{\lambda 2}. \tag{18}$$

Now, Equation (16) can be expressed by combining Equations (17) and (18). Therefore, the ratio can be calculated directly from the light received at the fingertip and follows:

$$R = \frac{\Delta \left[\log \frac{I_0}{I} \right]_{\lambda 2}}{\Delta \left[\log \frac{I_0}{I} \right]_{\lambda 1}} = \frac{\left[\log \frac{I_0(d1)}{I(d1)} - \log \frac{I_0(d2)}{I(d2)} \right]_{\lambda 2}}{\left[\log \frac{I_0(d1)}{I(d1)} - \log \frac{I_0(d2)}{I(d2)} \right]_{\lambda 1}} = \frac{\left[\log \frac{I(d1)}{I(d2)} \right]_{\lambda 2}}{\left[\log \frac{I(d1)}{I(d2)} \right]_{\lambda 1}} \,. \tag{19}$$

Using Equations (10) and (11), we obtain

$$P_{HbO} = SpO_2 * (1 - P_{HbA1c}). \tag{20}$$

Equation (10) can be expressed in terms of SpO_2 and P_{HbA1c} as

$$\begin{aligned} P_{HHb} &= 1 - (P_{HbO} + P_{HbA1c}) \text{ and} \\ &= (1 - SpO_2) * (1 - P_{HbA1c}). \end{aligned} \tag{21}$$

Solving for the values of P_{HbO} and P_{HHb}, the following equation is obtained:

$$R = \frac{P_{HbA1c}[\varepsilon_{HbA1c}(\lambda 2) - \varepsilon_{HHb}(\lambda 2) \times (1- SpO_2) - \varepsilon_{HbO}(\lambda 2) \times SpO_2] + [\varepsilon_{HHb}(\lambda 2) \times (1- SpO_2) + \varepsilon_{HbO}(\lambda 2) \times SpO_2]}{P_{HbA1c}[\varepsilon_{HbA1c}(\lambda 1) - \varepsilon_{HHb}(\lambda 1) \times (1- SpO_2) - \varepsilon_{HbO}(\lambda 1) \times SpO_2] + [\varepsilon_{HHb}(\lambda 1) \times (1- SpO_2) + \varepsilon_{HbO}(\lambda 1) \times SpO_2]}, \tag{22}$$

or

$$P_{HbA1c} = \frac{[\varepsilon_{HHb}(\lambda 2) \times (1- SpO_2) + \varepsilon_{HbO}(\lambda 2) \times SpO_2] - R[\varepsilon_{HHb}(\lambda 1) \times (1- SpO_2) + \varepsilon_{HbO}(\lambda 1) \times SpO_2]}{R[\varepsilon_{HbA1c}(\lambda 1) - \varepsilon_{HHb}(\lambda 1) \times (1- SpO_2) - \varepsilon_{HbO}(\lambda 1) \times SpO_2] - [\varepsilon_{HbA1c}(\lambda 2) - \varepsilon_{HHb}(\lambda 2) \times (1- SpO_2) - \varepsilon_{HbO}(\lambda 2) \times SpO_2]}. \tag{23}$$

The values of the molar absorption coefficients of *HbA1c*, *HbO*, and *HHb* for the two different wavelengths (525 and 615 nm) are given in Table 1. The molar absorption coefficients of *HbA1c* were taken from Hossain et al. [16] and those of *HbO* and *HHb* were considered from [17].

Table 1. Molar absorption coefficients for the blood vessel model.

Substance	Molar Absorption Coefficient ($cm^{-1} \cdot M^{-1}$)	
	$\lambda 1$ = 525 nm	$\lambda 2$ = 615 nm
HbA1c	455,139.5677	170,555.4218
HbO	30,882.8	1166.4
HHb	35,170.8	7553.4

2.2.2. Whole Finger Model

The whole finger model considers the lumped fingertip constituents as a homogeneous mixture. The blood entering this model will increase the fractional volume of arterial blood. Considering only the increase in the arterial fraction, the equation for the absorption coefficient becomes [14]:

$$C_a = \left(V_a \mu_a^{art}(\lambda) + V_v \mu_a^{vein}(\lambda) + V_w \mu_a^{water}(\lambda) + (1 - (V_a + V_v + V_w)\right) \times \mu_a^{baseline}). \tag{24}$$

Equations (25) and (26) can be easily obtained [14] after replacing the values of P_{HbO} and P_{HHb} from Equations (20) and (21), as follows:

$$\mu_a^{art} = \left\{P_{HbA1c}\left(\mu_a^{HbA1c}(\lambda) - \mu_a^{HbO}(\lambda) SpO_2 - \mu_a^{HHb}(\lambda)(1 - SpO_2)\right) + \mu_a^{HbO}(\lambda) SpO_2 + \mu_a^{HHb}(\lambda)(1 - SpO_2)\right\} \text{ and} \tag{25}$$

$$\mu_a^{vein} = \left\{P_{HbA1c}\left(\mu_a^{HbA1c}(\lambda) - \mu_a^{HbO}(\lambda) SpO_2 - \mu_a^{HHb}(\lambda)(1 - SpO_2)\right) + \mu_a^{HbO}(\lambda) SpO_2 + \mu_a^{HHb}(\lambda)(1 - SpO_2)\right\}. \tag{26}$$

Now, considering the arterial fraction increment, the absorption coefficient equation is as shown in Equation (27). Here, ΔC_a represents the change in the absorption coefficient due to a change in the arterial blood volume:

$$C_a + \Delta C_a = \left((V_a + \Delta V_a)\mu_a^{art}(\lambda) + V_v \mu_a^{vein}(\lambda) + V_w \mu_a^{water}(\lambda) + (1 - (V_a + \Delta V_a + V_v + V_w)\right) \times \mu_a^{baseline}). \tag{27}$$

After subtracting Equation (24) from (27), we obtain

$$\Delta C_a = \Delta V_a(\mu_a^{art}(\lambda) - \mu_a^{baseline}(\lambda)). \tag{28}$$

From the Beer–Lambert law, we obtain

$$I = I_o \times 10^{-C_a d}. \tag{29}$$

Equation (29) must be differentiated in terms of C_a to find the relationship between the physical light intensity and Equation (28):

$$\frac{dI}{dC_a} = -\ln(10) I_o d \times 10^{-C_a d} \text{ and} \tag{30}$$

$$\frac{dI}{dC_a} \approx \frac{\Delta I}{\Delta C_a}. \tag{31}$$

From Equations (30) and (31), we obtain

$$\Delta I \approx -\ln(10) I_o \Delta C_a d \times 10^{-C_a d}. \tag{32}$$

Now, the AC–DC intensity ratio is generated by the assumption $\frac{I_{AC}}{I_{DC}} = \frac{\Delta I}{I}$. Hence, dividing Equation (32) by Equation (29) provides

$$\frac{\Delta I}{I} \approx -\ln(10) \Delta V_a \left(\mu_a^{art}(\lambda) - \mu_a^{baseline}(\lambda) \right) d. \tag{33}$$

Thus, the ratio equation becomes

$$R = \frac{\left[\frac{\Delta I}{I}\right]_{\lambda_2}}{\left[\frac{\Delta I}{I}\right]_{\lambda_1}} = \frac{\mu_a^{art}(\lambda 2) - \mu_a^{baseline}(\lambda 2)}{\mu_a^{art}(\lambda 1) - \mu_a^{baseline}(\lambda 1)}. \tag{34}$$

After solving Equation (34) for P_{HbA1c}, we obtain Equation (35):

$$P_{HbA1c} = \frac{\mu_a^{HbO}(\lambda 2) \cdot SpO_2 + \mu_a^{HHb}(\lambda 2) \cdot (1 - SpO_2) - \mu_a^{baseline}(\lambda 2) - R \cdot \left(\mu_a^{HbO}(\lambda 2) \cdot SpO_2 + \mu_a^{HHb}(\lambda 2) \cdot (1 - SpO_2) - \mu_a^{baseline}(\lambda 2) \right)}{R \cdot \left(\mu_a^{HbA1c}(\lambda 1) - \mu_a^{HbO}(\lambda 1) \cdot SpO_2 - \mu_a^{HHb}(\lambda 1) \cdot (1 - SpO_2) \right) - \left(\mu_a^{HbA1c}(\lambda 1) - \mu_a^{HbO}(\lambda 1) \cdot SpO_2 - \mu_a^{HHb}(\lambda 1) \cdot (1 - SpO_2) \right)}. \tag{35}$$

The values of the molar absorption coefficients of *HbA1c*, *HbO*, *HHb*, skin baseline, and water for the two wavelengths (525 and 615 nm) are given in Table 2. The molar absorption coefficients of *HbA1c*, *HbO*, and *HHb* were considered from the study mentioned before, and the skin baseline and water values were considered from the studies by Saidi [18] and Segelstein [19], respectively.

Table 2. Absorption coefficients for the whole finger model.

Substance	Absorption Coefficient (cm^{-1})	
	$\lambda 1$ = 525 nm	**$\lambda 2$ = 615 nm**
HbA1c	1058.4641	396.6405
HbO	71.8205	2.7126
HHb	81.7926	17.566
Skin Baseline	1.0966	0.6552
Water	0.0003927	0.0027167

2.3. SpO_2 Calculation

To calculate the SpO_2 values from the PPG signals, we followed the method in [20]. The ratio R_{SpO_2} was calculated from the ratio of the normalized intensity of the received green light ($I_{n_{\lambda 1}}$) to red light ($I_{n_{\lambda 2}}$), which is expressed as Equation (24):

$$R_{SpO_2} = \frac{\Delta A_{\lambda 2}}{\Delta A_{\lambda 1}} = \frac{ln(I_{n_{\lambda 2}})}{ln(I_{n_{\lambda 1}})}. \tag{36}$$

As light passes through the additional optical path Δd at systole, from Equation (11), it is written as

$$d_1 = d_2 + \Delta d. \tag{37}$$

The normalized intensity of the received light at wavelength λ can be expressed as

$$I_{n_\lambda} = \frac{I}{I_{H_{d_2}}}, \tag{38}$$

where I represents the light intensity received by the photodetector (PD) and $I_{H_{d2}}$ represents the highest intensity at diastole. The absorbance at wavelength λ can be found using the concentrations of oxyhemoglobin and deoxyhemoglobin as follows:

$$\Delta A_\lambda = (\varepsilon_{HbO}(\lambda) \times c_{HbO} + \varepsilon_{HHb}(\lambda) \times c_{HHb}) \times \Delta d. \tag{39}$$

Now, replacing c_{HbO} and c_{HHb} in Equation (39) using Equation (4), we obtain

$$\begin{aligned} \Delta A_\lambda &= (\varepsilon_{HbO}(\lambda) \times SpO_2(c_{HbO} + c_{HHb}) + \varepsilon_{HHb}(\lambda)(1 - SpO_2)(c_{HbO} + c_{HHb})) \times \Delta d \text{ or} \\ \Delta A_\lambda &= (\varepsilon_{HbO}(\lambda) \times SpO_2 + \varepsilon_{HHb}(\lambda)(1 - SpO_2)) \times (c_{HbO} + c_{HHb}) \times \Delta d. \end{aligned} \tag{40}$$

Now, (36) can be expressed as

$$R_{SpO_2} = \frac{\Delta A_{\lambda 2}}{\Delta A_{\lambda 1}} = \frac{(\varepsilon_{HbO}(\lambda 2) \times SpO_2 + \varepsilon_{HHb}(\lambda 2)(1 - SpO_2)) \times (c_{HbO} + c_{HHb})}{(\varepsilon_{HbO}(\lambda 1) \times SpO_2 + \varepsilon_{HHb}(\lambda 1)(1 - SpO_2)) \times (c_{HbO} + c_{HHb})}. \tag{41}$$

Finally, the oxygen saturation (SpO_2) can be calculated as

$$SpO_2 = \frac{\varepsilon_{HHb}(\lambda 2) - (\varepsilon_{HHb}(\lambda 1) \times R_{SpO_2})}{(\varepsilon_{HHb}(\lambda 2) - \varepsilon_{HbO}(\lambda 2)) + (\varepsilon_{HbO}(\lambda 1) - \varepsilon_{HHb}(\lambda 1) \times R_{SpO_2})}. \tag{42}$$

3. Methodology

To estimate the *HbA1c* value noninvasively, in this study, two different ratio calibrations were applied. Each ratio equation used for the calibration of the SpO_2 and *HbA1c* estimation is defined differently. In the ratio calibration, two XGBoost models were used for calibrating the ratio values for estimating SpO_2 and *HbA1c*. If necessary, value (*HbA1c*) calibration can be used in addition to ratio calibrations to improve the accuracy. We note that value (*HbA1c*) calibration can be optionally adopted when the desired performance cannot be achieved with only ratio calibrations.

3.1. Dataset-Related Information

To evaluate the accuracy of the model and validity of the theory, we proceeded using the same data from the 20 subjects noted in [14]. Of these, thirteen were prediabetic, three were diabetic, and four were normal. The participants ranged in age from 25 to 55 (31.6 ± 10) years. Five of the subjects were female and fifteen were male. The mean and standard deviation (SD) of the finger widths and BMIs in the dataset were 1.30 ± 0.13 and 28.86 ± 3.74, respectively.

In this study, devices such as the Schiller Argus OXM Plus and invasive Bio-Hermes A1C EZ 2.0 were used to collect the $\%SpO_2$ and the data on the National Glycohemoglobin Standardization Program (NGSP) $\%HbA1c$ levels, respectively. The study also involved recording a 4 min PPG signal, with 2 min being transmissive and the remaining 2 min being reflective measurements. The transmissive PPG signal was chosen for the study as it aligned with the theoretical derivation used in the research.

The Institutional Review Board (IRB) of Kookmin University in Seoul, Korea, provided guidelines for the study protocol. The IRB procedures of Kookmin University were followed in conducting this study. Additionally, all participants gave their permission in advance for the data to be used academically. More details on the clinical dataset information can be found in [14]. Statistical summaries of the entire dataset used in this study are shown in Figure 2 and Table 3.

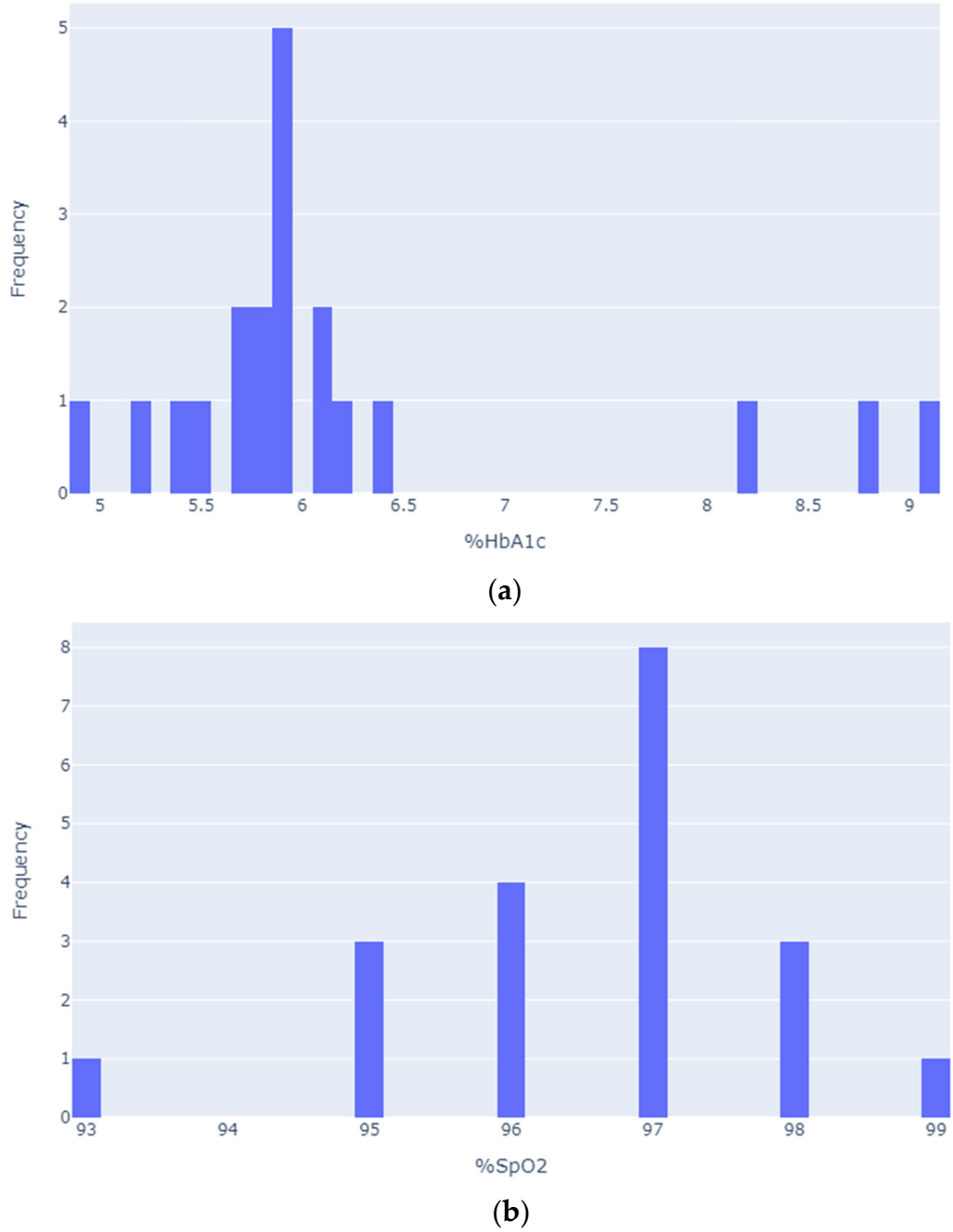

Figure 2. Histograms of the measured dataset: (**a**) %NGSP *HbA1c* and (**b**) $\%SpO_2$ values.

Table 3. Statistics of the measured $\%HbA1c$ and $\%SpO_2$ data.

	Min	Max	Mean	Median	SD	Variance	25th Percentile	75th Percentile
$\%HbA1c$	4.9	9.1	6.224	5.9	1.0308	1.0626	5.7	6.2
$\%SpO_2$	93	99	96.6	97.0	1.4142	2.0	96.0	97.0

3.2. Proposed Method: HbA1c *Estimation Using Only Two Wavelengths*

A workflow diagram of the proposed method is shown in Figure 3.

Data acquisition and data preprocessing were performed similar to [14]. For data acquisition, we used the commercial sensor module DFRobot SEN0212 comprising a color sensor (TCS34725) and a set of four white LEDs [14]. TCS34725 is a highly sensitive sensor

with three wavelengths (465, 525, and 615 nm). Although the device used here could capture both the transmissive and reflective signals of all three wavelengths, only the transmissive signals of two wavelengths (525 and 615 nm) were considered in this study. The PPG waveform was then preprocessed by filtering through a second-order Butterworth lowpass filter with a cutoff frequency of 8 Hz. As can be seen in Figure 3, two XGBoost calibration models were used here for the ratio calibrations of SpO_2 and *HbA1c*. We note that in [14], the SpO_2 and *HbA1c* estimates were obtained by simultaneously performing two ratio calibrations using three wavelengths, whereas in this study, the different ratio calibrations were separately performed using only two wavelengths to obtain the SpO_2 and *HbA1c* estimates sequentially.

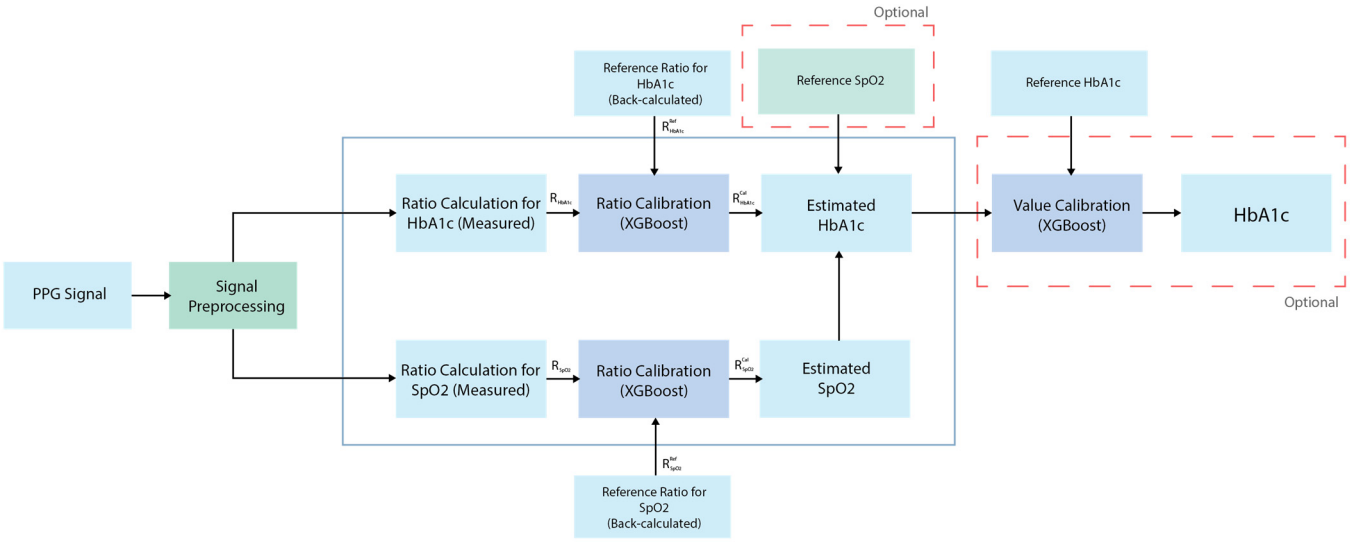

Figure 3. *HbA1c* estimation using only two wavelengths.

3.3. Calibration

Calibration was performed after the dataset creation and data preprocessing. For this reason, first the ratio values were calculated directly from the input intensity values. The ratio value for SpO_2 was calculated using Equation (36) from the input PPG signals. The ratio values for *HbA1c* were calculated using Equations (19) and (34) for the blood vessel and whole finger models, respectively. Then, the reference ratio values for SpO_2 were inversely calculated from the reference SpO_2 values using Equation (42). The reference ratio values for *HbA1c* were also inversely calculated in a similar way using Equations (23) and (35) for the blood vessel and whole finger models, respectively. This process of calibrating the ratio values was essential because different people have different finger widths and skin and fat layer qualities. This calibration method is used to reduce the effects of skin, fat layer, and finger widths on the PPG signal amplitude. When performing the calibration, the inputs are the ratio values calculated directly from the PPG signal and the corresponding finger widths and BMIs, while the target (reference) values are inversely calculated from the reference *HbA1c* values. The calibrated ratio values are then used to estimate the SpO_2 and *HbA1c* values. Here, to obtain the *HbA1c* estimated value, the estimated SpO_2 value was applied, and if the reference SpO_2 value was available, this reference value could be used instead of the SpO_2 estimate. After the ratio calibrations, additional value (*HbA1c*) calibrations could be conducted, if necessary. In the value calibrations, the *HbA1c* values estimated from the ratio calibration models could be further calibrated to improve the performance. Finger widths and BMIs were also considered as features in this case.

For the calibration, the XGBoost model was used. The leave-one-out cross validation (LOOCV) approach was implemented to evaluate the calibration results. LOOCV is a technique for evaluating a machine learning model's performance. In the LOOCV technique, the model is trained on all but one of the data points before being evaluated on the remaining data point. This procedure is repeated for each data point, with each point serving as the test set exactly once. The model's overall performance is then determined by averaging the performances of all iterations. LOOCV is a special case of the k-fold cross-validation, where k is equal to the number of data points. As we focused on estimating *HbA1c* from the PPG signals using the Beer–Lambert-based model, implementing LOOCV in the regression was reliable and unbiased for achieving the desired model performance.

4. Results and Discussion

4.1. Blood Vessel Model

After performing the ratio calibrations, Clarke's error-grid analysis (EGA) [20,21] and Bland–Altman analysis plots were used for the performance analysis of the estimated *HbA1c* values. As seen in Figure 4, from the EGA, Zone A contained 15 samples (75%; clinically accurate), Zone B contained 5 samples (25%; data outside of 20% of the reference but would not lead to inappropriate treatment), and Zone C contained 0 samples (0%; data that would lead to inappropriate treatment). The Bland–Altman analysis indicated that the blood vessel model provided a bias of -0.15998 ± 0.961, and the limits of agreement ranged from -1.12 to 0.80. For the estimated %*HbA1c* values, statistical analysis using mean square error (MSE), mean error (ME), mean absolute deviation (MAD), root mean square error (RMSE), and Pearson's r yielded 0.266, -0.1599, 0.423, 0.5156, and 0.8959, respectively.

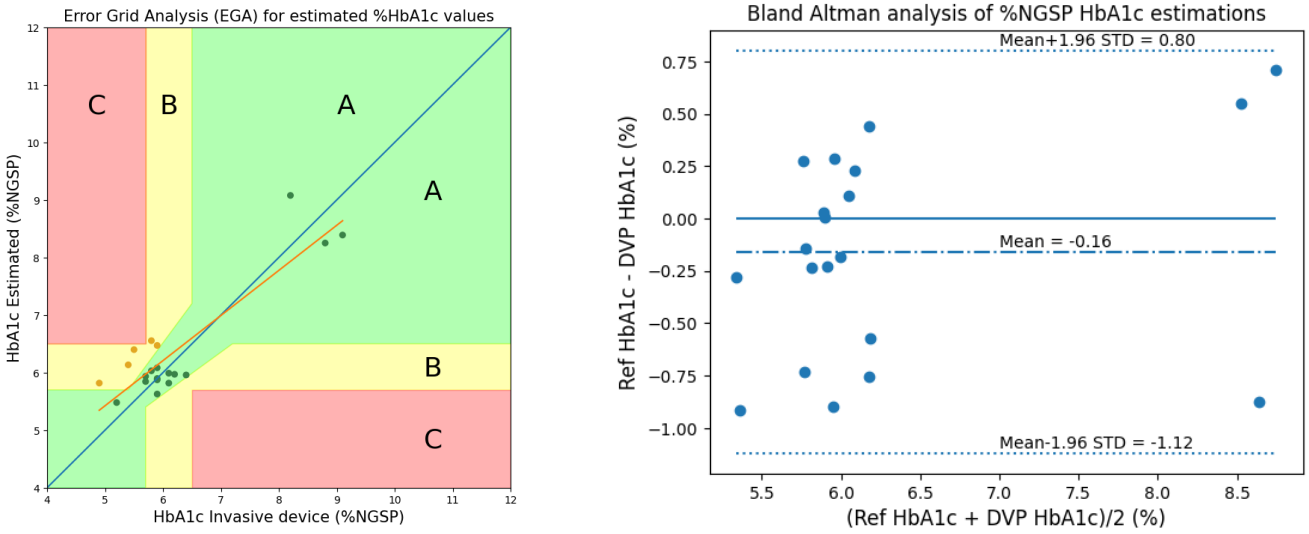

Figure 4. EGA and Bland–Altman analysis for the *HbA1c* estimation with the blood vessel model (considering ratio calibrations only).

We considered value (*HbA1c*) calibrations in addition to ratio calibrations, and the EGA and Bland–Altman analysis results are shown in Figure 5. From the EGA, Zone A contained 17 samples (85%), Zone B contained 3 samples (15%), and Zone C contained 0 samples (0%). The Bland–Altman analysis indicated that the blood vessel model provided a bias of -0.029 ± 0.8598, and the limits of agreement ranged from -0.89 to 0.83. For the estimated %*HbA1c* values, statistical analysis using MSE, ME, MAD, RMSE, and Pearson's r yielded 0.259, -0.0118, 0.4366, 0.5087, and 0.8873, respectively.

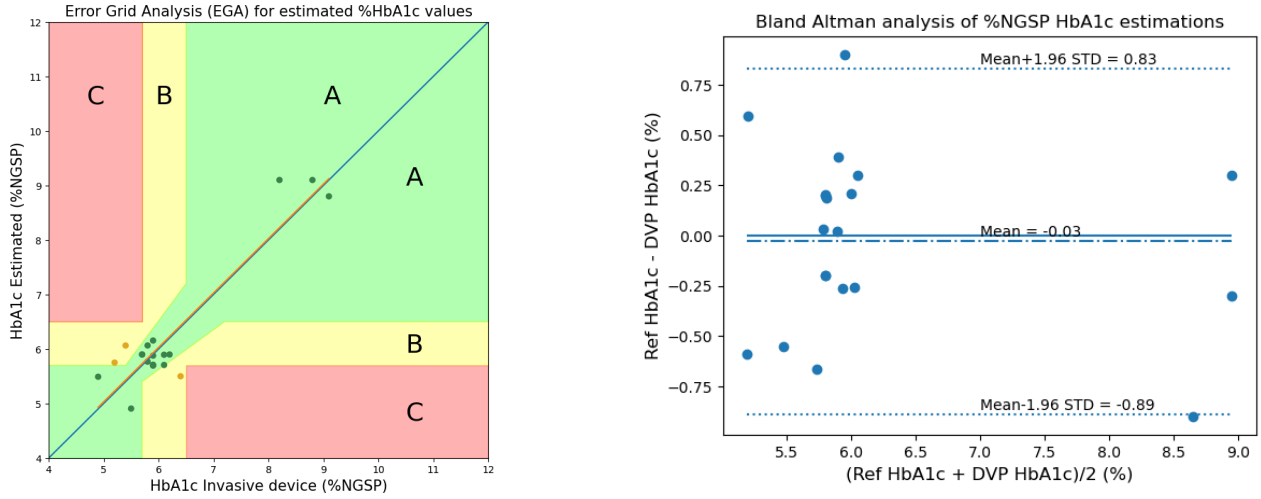

Figure 5. EGA and Bland–Altman analysis for the *HbA1c* estimation with the blood vessel model (considering both ratio and value calibrations).

4.2. Whole Finger Model

After performing the ratio calibrations considering the whole finger model, the results are shown in Figure 6; from the EGA, Zone A contained 16 samples (80%), Zone B contained 4 samples (20%), and Zone C contained 0 samples (0%). The Bland–Altman analysis indicated that the bias was -0.0718 ± 0.9260, and the limits of agreement ranged from -1.00 to 0.85. The limits of agreement of the whole finger model were smaller than those of the blood vessel model. For the estimated %*HbA1c* values, statistical analysis using MSE, ME, MAD, RMSE, and Pearson's r yielded 0.224, -0.0559, 0.3914, 0.4736, and 0.9052, respectively.

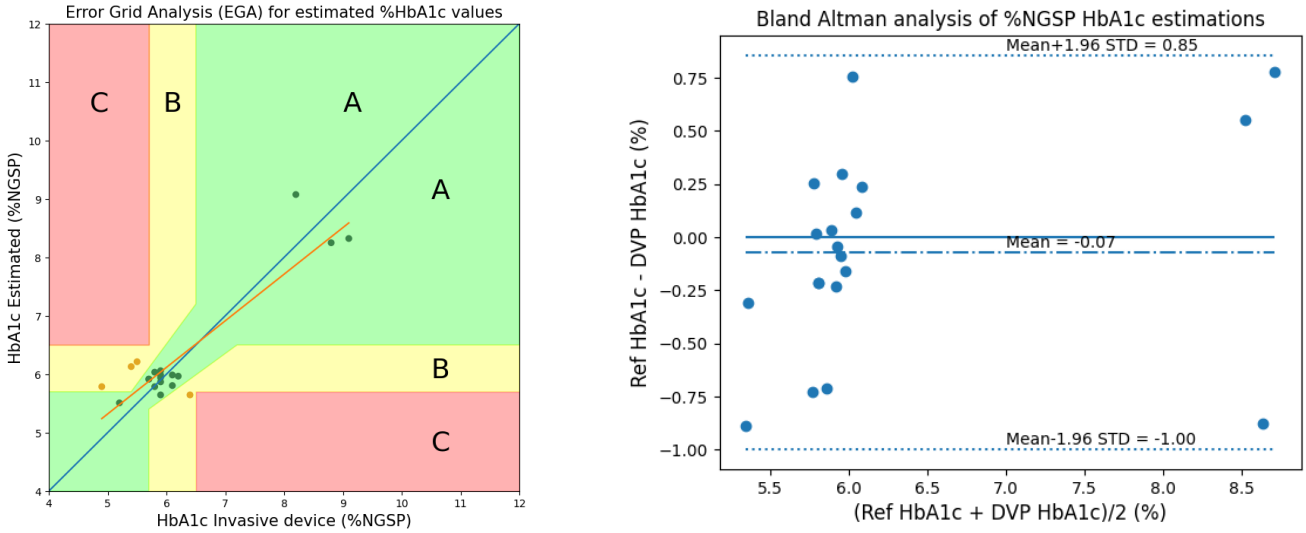

Figure 6. EGA and Bland–Altman analysis for *HbA1c* with the whole finger model (considering ratio calibrations only).

We considered value (*HbA1c*) calibrations in addition to ratio calibrations, and the EGA and Bland–Altman analysis results are shown in Figure 7. From the EGA, Zone A contained 17 samples (85%), Zone B contained 3 samples (15%), and Zone C contained 0 samples (0%). The Bland–Altman analysis indicated that the bias was 0.0066 ± 0.8623, and the limits of agreement ranged from -0.86 to 0.87. For the estimated %*HbA1c* values, statistical analysis using MSE, ME, MAD, RMSE, and Pearson's r yielded 0.194, 0.0066, 0.3662, 0.4400, and 0.9296, respectively.

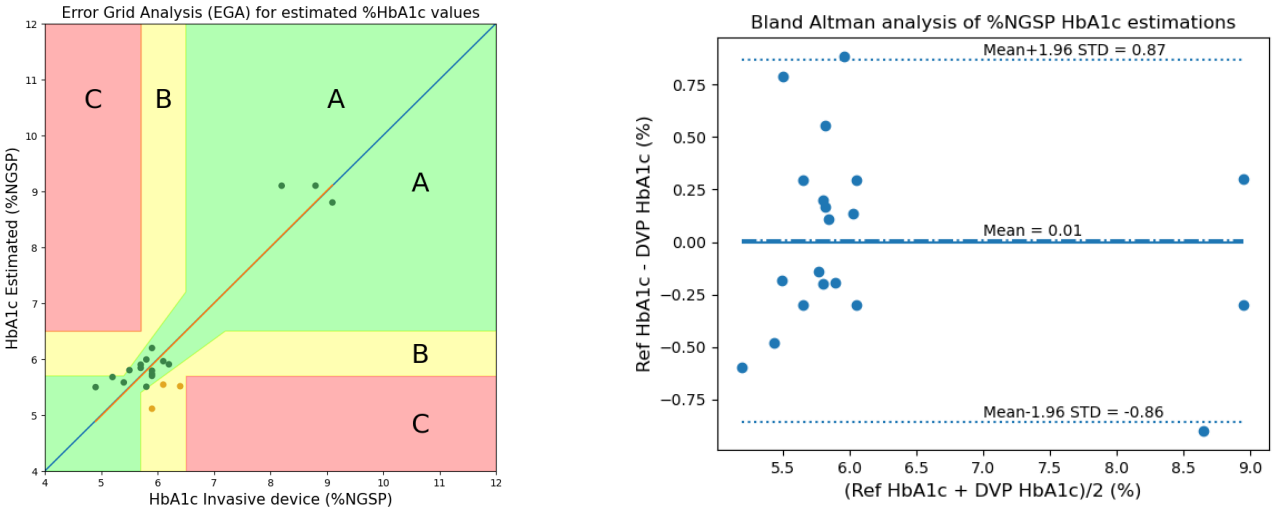

Figure 7. EGA and Bland–Altman analysis for *HbA1c* with the whole finger model (considering both ratio and value calibrations).

4.3. SpO_2 Estimation

For the estimated SpO_2 values obtained through the ratio calibration, the scatter plot and Bland–Altman analysis results are plotted in Figure 8. The Bland–Altman analysis provided a bias of -0.0894 ± 3.293, and the limits of agreement ranged from -3.38 to 3.20. For the estimated $\%SpO_2$ values, statistical analysis using MSE, ME, MAD, and RMSE yielded 2.831, -0.089, 1.392, and 1.683, respectively. The reference closeness factor (RCF), defined as Equation (43), was found to be 0.986, as shown below:

$$RCF = \frac{1}{N}\sum_{i=1}^{N}\left(1 - \frac{\left|SpO_2^{Ref}(i) - SpO_2^{Est}(i)\right|}{100}\right). \quad (43)$$

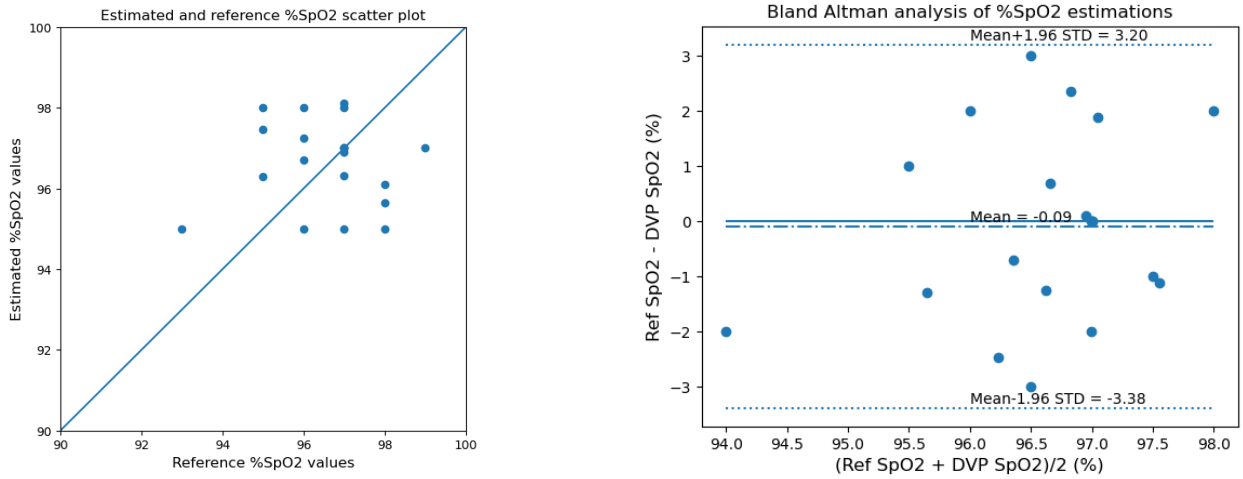

Figure 8. Scatter plot and Bland–Altman analysis for the estimated SpO_2 values after ratio calibration.

4.4. Performance Comparisons Using the Evaluation Metrics

Table 4 shows the performance comparison results for the accuracy of the *HbA1c* estimates between the previous study [14] using three wavelengths and this study using only two wavelengths. We can see that in the *HbA1c* estimation, even though only two wavelengths were used, the performance was comparable to (though slightly worse than) that of the previous study when only ratio calibrations were applied, and when value

(*HbA1c*) calibration was applied in addition to ratio calibrations, the performance was almost equal to or slightly better compared to that of the previous study [14].

Table 4. *HbA1c* estimation performance comparison between this study and the previous study.

Method \ Metric	MSE	ME	MAD	RMSE	Pearson's r
Blood vessel [14]	0.211	−0.031	0.375	0.459	0.916
Whole finger [14]	0.110	−0.065	0.271	0.332	0.959
Blood vessel (Proposed1)	0.266	−0.159	0.423	0.515	0.896
Whole finger (Proposed1)	0.224	−0.055	0.391	0.473	0.905
Blood vessel (Proposed2)	0.193	−0.029	0.363	0.439	0.929
Whole finger (Proposed2)	0.194	0.007	0.366	0.440	0.930

Proposed1: using ratio calibrations only; Proposed2: using both ratio calibrations and value (*HbA1c*) calibrations.

Table 5 shows the EGA-based comparison between the previous study [14] for estimating *HbA1c* using three wavelengths and this study using only two wavelengths. The number inside the table indicates the number of points (%values inside bracket) in the corresponding zone. For the whole finger model, the performances of Proposed1 and Proposed2 were similar. However, for the blood vessel model, the performance of Proposed2 was slightly better, with 80% of the data points inside Zone A. Compared with the previous study [14], the Proposed2 method performed better.

Table 5. EGA-based comparison between this study and the previous study.

Method \ Zone	A	B	C
Blood vessel [14]	15 (75)	5 (25)	0 (0)
Whole finger [14]	18 (90)	2 (10)	0 (0)
Blood vessel (Proposed1)	15 (75)	5 (25)	0 (0)
Whole finger (Proposed1)	17 (85)	3 (15)	0 (0)
Blood vessel (Proposed2)	16 (80)	4 (20)	0 (0)
Whole finger (Proposed2)	17 (85)	3 (15)	0 (0)

Proposed1: using ratio calibrations only; Proposed2: using both ratio calibrations and value (*HbA1c*) calibrations.

Table 6 summarizes the Bland–Altman-analysis-based comparison between the previous study [14] for estimating *HbA1c* using three wavelengths and this study using only two wavelengths. We can see that the limits of agreement for the proposed methods are not very different compared to those of the previous method [14]. The 95% limits of agreement should contain the difference between the estimates and the reference for 95% of the measurements. In the previous study [14], considering the whole finger model, only one data point was found outside this limit. Similarly, in the proposed method here, there was only one data point outside the limit.

Table 6. Bland-Altman-analysis-based comparison between this study and the previous study for estimating *HbA1c*.

Method \ Metric	Bias	Limit of Agreement (95%; 1.96 SD)	Data Points Out of Limit of Agreement
Blood vessel [14]	-0.03 ± 0.458	−0.93 to 0.87	0
Whole finger [14]	-0.06 ± 0.326	−0.70 to 0.57	1
Blood vessel (Proposed1)	-0.16 ± 0.961	−1.12 to 0.80	0
Whole finger (Proposed1)	-0.072 ± 0.926	−1.00 to 0.85	0
Blood vessel (Proposed2)	-0.029 ± 0.859	−0.89 to 0.83	1
Whole finger (Proposed2)	-0.0066 ± 0.862	−0.86 to 0.87	1

Proposed1: using ratio calibrations only; Proposed2: using both ratio calibrations and value (*HbA1c*) calibrations.

The SpO_2 estimation performance comparison using the evaluation metrics is summarized in Table 7. We can see from Table 7 that the RCF score of SpO_2 estimated in this study was almost the same as that of the previous study (whole finger). Considering other statistical analyses, we can see that the overall performance of the SpO_2 estimation in this study was slightly better compared to that of the previous study [14].

Table 7. SpO_2 estimation performance comparison between this study and the previous study.

Method \ Metric	MSE	ME	MAD	RMSE	RCF
Previous (blood vessel) [14]	4.038	0.178	1.676	2.010	0.983
Previous (whole finger) [14]	2.924	−0.246	1.395	1.710	0.986
Proposed	2.831	−0.089	1.392	1.683	0.986

Table 8 summarizes the comparisons based on the Bland–Altman analysis between the previous study [14] and this study in estimating SpO_2. From this, it is clear that the proposed method performed well in comparison with the previous study.

Table 8. Bland-Altman-analysis-based comparison between this study and the previous study for estimating SpO_2.

Method \ Metric	Bias	Limit of Agreement (95%; 1.96 SD)	Data Points Out of Limit of Agreement
Previous (blood vessel) [14]	-0.178 ± 2.002	−3.74 to 4.10	0
Previous (whole finger) [14]	-0.246 ± 1.690	−3.56 to 3.07	0
Proposed	-0.0894 ± 3.293	−3.38 to 3.20	0

5. Conclusions

In this study, we used the Beer–Lambert law to estimate *HbA1c* noninvasively from the fingertip by considering only two wavelengths. In our previous work [14], three wavelengths were used, which made the system relatively complex. Obtaining nearly the same performance, as seen from Table 4, while reducing complexity was the main contribution of this study. To this end, two ratio calibrations were used to obtain results comparable to those of the previous study. In the ratio calibrations, two XGBoost models were used: one for SpO_2 and the other for *HbA1c*. The Pearson's r values for the estimated *HbA1c* values were 0.896 and 0.905 considering the ratio calibrations with the blood vessel and whole finger models, respectively.

When value (*HbA1c*) calibrations were applied in addition to ratio calibrations, we could further improve the performance, and the Pearson's r values of the estimated *HbA1c* levels were 0.929 and 0.930 for the blood vessel and whole finger models, respectively. Further, as in the previous study, the whole finger model performed slightly better than the blood vessel model, as shown in Table 4. We also showed that the RCF score of SpO_2 estimated in this study was nearly the same as that of the previous study (whole finger model).

We expect that further studies using larger datasets and deep learning techniques can improve these results. The performance can also be improved by calibration in a more controlled manner, paying more attention to factors such as light scattering, finger-width variability, and data filtering. We also note that there is considerable potential for further research on the noninvasive estimation of *HbA1c*.

Author Contributions: M.S.T.: conceptualization, methodology, software, and writing—original draft; T.-H.K.: formal analysis; H.K.: resources and validation; K.-D.K.: validation, supervision, project administration, and funding acquisition. All authors have read and agreed to the published version of the manuscript.

Funding: This work was supported by the National Research Foundation (NRF) of Korea, funded by the Ministry of Science and ICT (2022R1A5A7000765), and it was also supported by the Basic Science Research Program through the National Research Foundation (NRF) of Korea, funded by the Ministry of Education (NRF-2022R1A2C2010298). This research was also supported through the Korea Industrial Technology Association (KOITA), funded by the Ministry of Science and ICT (MSIT).

Institutional Review Board Statement: All protocols and procedures in this study were approved by the Institutional Review Board (IRB) of Kookmin University, Seoul, Republic of Korea (approval date: 17 July 2020). The procedures followed the Helsinki Declaration of 1975, as revised in 2008. All human participants agreed in advance to participate and share their data for academic research purposes. The IRB protocol number is: KMU-202006-HR-237.

Informed Consent Statement: Informed consent was obtained from all subjects involved in the study.

Data Availability Statement: We have created our own dataset for this study. Since further research is underway, we are unable to publish the dataset at present.

Conflicts of Interest: The authors declare that they have no conflict of interest. The funders had no role in the design of the study; in the collection, analyses, or interpretation of the data; in the writing of the manuscript; or in the publication of the results.

Appendix A

The hardware device that we implemented provides three wavelengths (465, 525, and 615 nm), and we would like to provide a rationale for the selection of two out of the three wavelengths. For selecting the proper wavelength pair, M_h and M_s were calculated using Equations (A1) and (A2) according to [21]. The wavelengths used here are 465 nm (blue), 525 nm (green), and 615 nm (red). These results are summarized in Table A1.

$$M_h = \frac{\sum_{i=1}^{2} \frac{dR_i}{dHbA1c}}{2} \tag{A1}$$

$$M_s = \frac{\sum_{i=1}^{2} \frac{dR_i}{dSpO_2}}{2} \tag{A2}$$

Table A1. M_h and M_s statistics.

	Blood Vessel Model			**Whole Finger Model**		
	GR	**BR**	**BG**	**GR**	**BR**	**BG**
M_h	0.342204	0.45122	0.03224	0.34758	0.39087	0.00068
M_s	1.964076	1.95179	1.97210	1.93640	0.19509	0.31324

GR: Green-Red; BR: Blue-Red; BG: Blue-Green.

The larger M_h and M_s values, the more sensitive each wavelength pair is to changes in its parameters ($HbA1c$ and SpO_2). That is why the higher the values of M_h and M_s, the better the performance is. Table A1 shows that for the blue-red pair, both models have the highest M_h values, while the M_s values of both models are not good. For the blue-green pair, only the M_s value for blood vessel model is the best, but the rest are poor. Note that, in the case of the green-red pair, it can be seen that the overall result is relatively good.

Table A2 shows the results of the EGA-based comparison of *HbA1c* estimation for different wavelength pairs of the Proposed1 method. We can see that the green-red pair performs better than the other pairs since most of the data points were found in zone A for both blood vessel and whole finger models.

Table A2. EGA-based comparison of *HbA1c* estimation for different wavelength pairs.

Wavelength Pair	Metric / Method	A	B	C
GR	Blood vessel (Proposed1)	15 (75)	5 (25)	0 (0)
	Whole finger (Proposed1)	17 (85)	3 (15)	0 (0)
BR	Blood vessel (Proposed1)	14 (70)	6 (30)	0 (0)
	Whole finger (Proposed1)	15 (75)	5 (25)	0 (0)
BG	Blood vessel (Proposed1)	12 (60)	7 (35)	1 (5)
	Whole finger (Proposed1)	14 (70)	6 (30)	0 (0)

References

1. Tapp, R.J.; Tikellis, G.; Wong, T.Y.; Harper, C.A.; Zimmet, P.Z.; Shaw, J.E.; on Behalf of the Australian Diabetes Obesity and Lifestyle Study Group. Longitudinal Association of Glucose Metabolism with Retinopathy Results from the Australian Diabetes Obesity and Lifestyle (AusDiab) Study. *Diabetes Care* **2008**, *31*, 1349–1354. [CrossRef] [PubMed]
2. Chen, C.; Xie, Q.; Yang, D.; Xiao, H.; Fu, Y.; Tan, Y.; Yao, S. Recent Advances in Electrochemical Glucose Biosensors: A Review. *RSC Adv.* **2013**, *3*, 4473–4491. [CrossRef]
3. Bandodkar, A.J.; Wang, J. Non-Invasive Wearable Electrochemical Sensors: A Review. *Trends Biotechnol.* **2014**, *32*, 363–371. [CrossRef] [PubMed]
4. Sharma, S.; Huang, Z.; Rogers, M.; Boutelle, M.; Cass, A.E.G. Evaluation of a Minimally Invasive Glucose Biosensor for Continuous Tissue Monitoring. *Anal. Bioanal. Chem.* **2016**, *408*, 8427–8435. [CrossRef] [PubMed]
5. Kagie, A.; Bishop, D.K.; Burdick, J.; la Belle, J.T.; Dymond, R.; Felder, R.; Wanga, J. Flexible Rolled Thick-Film Miniaturized Flow-Cell for Minimally Invasive Amperometric Sensing. *Electroanalysis* **2008**, *20*, 1610–1614. [CrossRef]
6. Li, M.; Bo, X.; Mu, Z.; Zhang, Y.; Guo, L. Electrodeposition of Nickel Oxide and Platinum Nanoparticles on Electrochemically Reduced Graphene Oxide Film as a Nonenzymatic Glucose Sensor. *Sens. Actuators B Chem.* **2014**, *192*, 261–268. [CrossRef]
7. Mandal, S.; Marie, M.; Kuchuk, A.; Manasreh, M.O.; Benamara, M. Sensitivity Enhancement in an In-Vitro Glucose Sensor Using Gold Nanoelectrode Ensembles. *J. Mater. Sci. Mater. Electron.* **2017**, *28*, 5452–5459. [CrossRef]
8. Little, R.R.; Roberts, W.L. A Review of Variant Hemoglobins Interfering with Hemoglobin A1c Measurement. *J. Diab. Sci. Technol.* **2009**, *3*, 446–451. [CrossRef] [PubMed]
9. Jeppsson, J.O.; Kobold, U.; Barr, J.; Finke, A.; Hoelzel, W.; Hoshino, T.; Miedema, K.; Mosca, A.; Mauri, P.; Paroni, R.; et al. Approved IFCC Reference Method for the Measurement of *HbA1c* in Human Blood. *Clin. Chem. Lab. Med.* **2002**, *40*, 78–89. [CrossRef] [PubMed]
10. Mandal, S.; Manasreh, M.O. An In-Vitro Optical Sensor Designed to Estimate Glycated Hemoglobin Levels. *Sensors* **2018**, *18*, 1084. [CrossRef] [PubMed]
11. Martín-Mateos, P.; Dornuf, F.; Duarte, B.; Hils, B.; Moreno-Oyervides, A.; Bonilla-Manrique, O.E.; Larcher, F.; Krozer, V.; Acedo, P. In-Vivo, Non-Invasive Detection of Hyperglycemic States in Animal Models Using Mm-Wave Spectroscopy. *Sci. Rep.* **2016**, *6*, 1–8. [CrossRef] [PubMed]
12. Usman, S.; Bani, N.A.; Kaidi, H.M.; Aris, S.A.M.; Jalil, S.Z.A.; Muhtazaruddin, M.N. Second Derivative and Contour Analysis of PPG for Diabetic Patients. In Proceedings of the 2018 IEEE EMBS Conference on Biomedical Engineering and Sciences, Sarawak, Malaysia, 3–6 December 2018; pp. 59–62. [CrossRef]
13. Saraoğlu, H.M.; Selvi, A.O. Determination of Glucose and *HbA1c* Values in Blood from Human Breath by Using Radial Basis Function Neural Network via Electronic Nose. In Proceedings of the National Biomedical Engineering Meeting, Istanbul, Turkey, 16–17 October 2014.
14. Hossain, S.; Sengupta, S.; Kwon, T.H.; Kim, K.D. Derivation and Validation of Gray-Box Models to Estimate Noninvasive in-Vivo Percentage Glycated Hemoglobin Using Digital Volume Pulse Waveform. *Sci. Rep.* **2021**, *11*, 12169. [CrossRef] [PubMed]
15. Yadav, J.; Rani, A.; Singh, V.; Murari, B.M. Prospects and Limitations of Non-Invasive Blood Glucose Monitoring Using near-Infrared Spectroscopy. *Biomed. Signal Process. Control* **2015**, *18*, 214–227. [CrossRef]
16. Hossain, S.; Satter, S.; Kwon, T.-H.; Kim, K.-D. Optical Measurement of Molar Absorption Coefficient of *HbA1c*: Comparison of Theoretical and Experimental Results. *Sensors* **2022**, *22*, 8179. [CrossRef] [PubMed]
17. Nishidate, I.; Yoshida, K.; Kawauchi, S.; Sato, S.; Sato, M. Tabulated Molar Extinction Coefficient for Hemoglobin in Water. *J. Jpn. Soc. Laser Surg. Med.* **1999**, *32*, 394–401. [CrossRef]
18. Saidi, I.S. Transcutaneous Optical Measurement of Hyperbilirubinemia in Neonates. Ph.D. Thesis, Rice University, Houston, TX, USA, 1992.

19. Segelstein, D.J. The Complex Refractive Index of Water. Ph.D. Thesis, University of Missouri, Kansas City, MO, USA, 1981.
20. Lochner, C.M.; Khan, Y.; Pierre, A.; Arias, A.C. All-Organic Optoelectronic Sensor for Pulse Oximetry. *Nat. Commun.* **2014**, *5*, 5745. [CrossRef] [PubMed]
21. Hossain, S.; Kim, K.-D. Comparison of Different Wavelengths for Estimating *HbA1c* and SpO_2 Noninvasively Using Beer-Lambert Law and Photon Diffusion Theory Derived Models. *J. Kor. Soc. Commun.* **2021**, *46*, 1301–1308. [CrossRef]